Numerical simulation of the crystal growth of Ti:Al₂O₃ material by the µ-PD Technology

H. Azoui[a], A. Laidoune[a], D. Haddad[b], D. Bahloul[a] and F. Merrouchi [c]

[a]*Département de Physique, Facultés des Sciences de la Matière ,Université de Batna1.*

1rue Chahid Boukhlouf Mohamed El-Hadi, 05000 Batna, Algeria.

[b]*Département de mécanique, Faculté de l'engineering, Laboratoire (LESEI), , Université de Batna2, Algeria.*

[c]*Département de. Hydraulique, Institut de génie civil, hydraulique et architecture, Université de Batna2.*

Abstract

In this work we have studied the growth of titanium doped sapphire using the micro-pulling down technique; we established a numerical, two-dimensional finite volume model in cylindrical coordinates with an axisymmetric configuration. The flow, the heat and the mass transfer are modeled by the differential equations of conservation of mass, momentum, energy and species. This problem, which takes into account the convection-diffusion coupling, is discretized using the Finite Volumes Method. Simulation results show that the longitudinal distribution of titanium remains homogeneous along the axis of the sapphire material. The radial mass transfer of titanium increases in the crystal when the pulling rate increases. This important result contributes to strengthen the coupling of the laser beam with the active ions and allows a highest laser output power. The melt/crystal interface for the µ-PD technique has a flat shape; this flatness of the interface shape agrees with the experiment observation and is very important since it shows that drawing conditions are very stable. Our model for the µ-PD method is in good agreement with experimental results.

Nomenclature

Bi Biotnumber, hR_d/k_m.

C dimensionless solute concentration.

C_0 initial solute concentration.

Cp_c specific heat capacity of the crystal (*J/KgK*).

Cp_m specific heat capacity of the melt (*J/KgK*).

D diffusion coefficient $\quad$ (m² /s).

g_0 gravitational acceleration $\quad$ (m² / s).

h heat transfer coefficient (w/cm² k⁻¹).

k_c thermal conductivity of crystal (w/m k).

k_m thermal conductivity of melt (w/m k).

Ma Marangoni number $((\partial\gamma/\partial T)\,R_dT_m)/(\mu_m\alpha_m)$.

Pe_c Peclect numbers of the crystal $\quad U_cR_d/\alpha_m$.

Pe_m Peclect numbers of the melt $\quad U_mR_d/\alpha_m$.

Pr Prandtl number $\quad \nu/\alpha_m$.

Ra_T thermal Rayleigh number

$g_0\beta_T(T_{max}-T_m)R_c^3/\alpha_m\nu$

Ra_S solutal Rayleigh number, $\quad \dfrac{g_0\beta_C C_0 R_c^3}{D}\nu$.

R_d crucible radius.

R_c crystal radius.

Sc Schmidt number, $\quad \nu_m/D$.

T dimensionless temperature.

T_a ambient temperature.

t time.

u r-component of velocity.

v z-component of velocity.

r dimensionless radial cylindrical coordinates.

z dimensionless axial cylindrical coordinates.

1. Introduction

Because of its exceptional chemical and physical properties [1], sapphire is a very important material used in several military, environmental, medical, and industrial applications [2,3]: optical systems, watch windows, cellular phone glasses, optical fibers, wave guides for surgery, needles for laser therapy and medical power delivery systems [2].

Titanium doped sapphire has excellent mechanical, thermal, and optical properties which allow the development of various systems especially laser devices [4]. Many growing techniques have been used to grow this material such as Czochralski (CZ) [5, 6], Heat exchanger method (HEM) [7] Kyroupolos (KY) [4] and pulsed laser deposition (PLD) [8, 9].

More recently there has been intense interest in using the micro-pulling-down method for the growth of shaped crystals fibers in a wide variety of domains, especially for laser, medical and optical application [10, 11].

The geometry, the shape and the quality of crystals play an important role in the choice of the growing technique [10]. We chose to study the micro pulling down technique because it allows the growth of stable high quality shaped crystals than the other comparable complex techniques [10]. In fact, it allows the control of the thermal gradient, the use of high pulling rates and high possibility to get stable shaped crystals [12]. Furthermore, when the pulling rate is sufficiently high the segregation problem can be avoided [2, 12].

The µ-PD technique now has become a major method for growing crystalline fibers of good quality [15] with controlled format imposed by the geometry of the capillary at the bottom of the crucible [10]. Because of the small amount of raw material, the µ-PD technique is used for research laboratories [2], especially to search for new materials.

In this work we have performed a numerical simulation of the growing process with the micro-pulling down µ-PD technique. The theoretical analysis of this method for the growth of single crystal fibers of Ti doped Al_2O_3 is conducted using the mass, momentum, energy and solutal concentration conservation laws.

The study of the problem is simplified to an incompressible flow of a viscous fluid in the molten zone governed by the Navier-Stokes, heat transfer and concentration equations under the Boussinesq approximation. We use a two-dimensional axisymmetric model discretized using a Finite Volumes Method (FVM) in cylindrical coordinates system(r, z).

The next section summarizes the growth conditions using the micro-pulling down technique. In Section 3 we present the mathematical formulation of our model that is the governing equations, the boundary conditions and the numerical scheme used in our simulations. Section 4 is devoted to the results and discussion, followed by conclusions in section 5.

2. Growth conditions
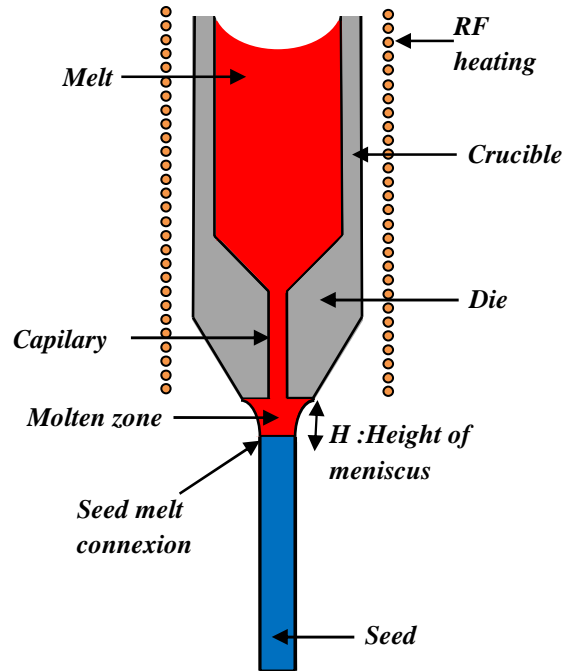
Fig.1 : Schematic diagram of domain of µ-PD.

The system to be modeled is sketched in Fig.1; the raw material (red color) in the crucible was heated until melting by using RF (Radio frequency) heating furnace [11]. The micro-pulling-down µ-PD uses a capillary die for the growth of shaped crystals.
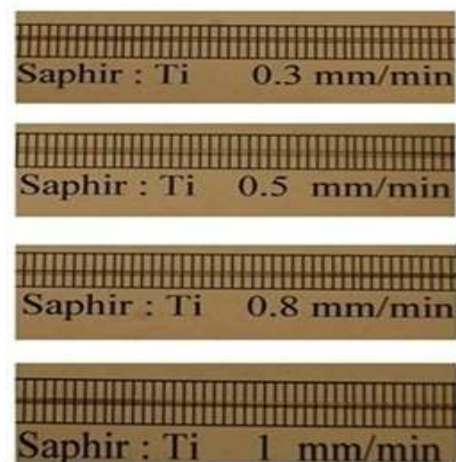
Fig.2. Ti doped sapphire fibers.

The growth is generated by the connection of the seed (blue color) with the drop at the bottom of the capillary die in the crucible. In Fig.2, we present titanium-doped sapphire crystal fibers along [0001] direction, for different pulling rates [19].

In order to perform the growth in steady conditions, many growth conditions have to be satisfied: Firstly; In order to grow the fiber with a constant diameter, the growth angle constraint needs to be specified [13]:

$$\frac{dR_m}{dz} = -\tan\phi_0 \qquad (1)$$

As shown in Fig. 3, R_m is the radial distance of the free surface, and ϕ_0 is the growth angle determined by crystallographic orientation and specified by the crystal-liquid-vapor triple junction [10].
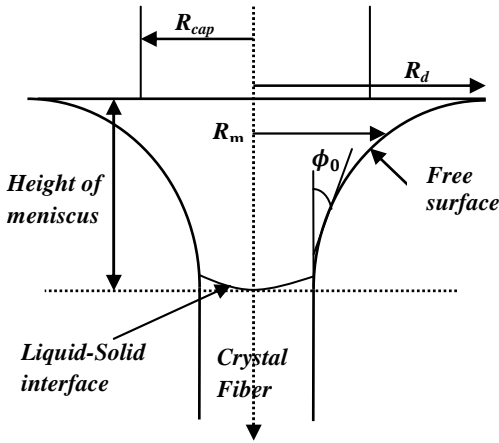

Fig.3: Zoom in the molten zone.

The crystal shape should be controlled by the shape of the meniscus (i.e., the $\phi = \phi_0$ requirement) [14].

In our case, for sapphire $\phi = \phi_0 = 17^0$ in the growth direction [0001] [12, 15].

The pulling is conducted down with controlled speed; equation (**2**) describes the relationship between the radius of the capillary, the radius of the crystal and the pulling rate [10].

$$\rho_m v_{cap} d_{cap}^2 = \rho_c d_c^2 v_c \qquad (2)$$

This equation states out the mass conservation between the inlet in the capillary and the outlet at the bottom of liquid-solid interface. The fundamental parameters involved in the micro-pulling down method [10] are:

the growth velocity v_c, the flow velocity at the capillary v_{cap}, the crucible radius at the bottom R_d, and the radius of the crystal $R_c = d_c/2$; while d_c and d_{cap} are the diameters of the growing crystal and the capillary respectively (fig.4).

The other parameter is the molten zone height; the relationship between these three parameters is theoretically given in [10] by:

$$H = R_c \cos\phi_0 \left[\csc\left(\frac{R_d}{R_c\cos\phi_0}\right) - \csc\left(\frac{1}{\cos\phi_0}\right) \right] (3)$$

The most important parameter determining the quality and uniformity of the obtained crystals [11] is the shape of the molten zone; where its meniscus profile, is given in [10, 16] by:

$$z(r) = R_c \cos\phi_0 \left[\csc\left(\frac{R_d}{R_c\cos\phi_0}\right) - \csc\left(\frac{r}{R_c\cos\phi_0}\right) \right] \quad (4)$$

Where r is the radial distance from the growth axis:

$$R_c \leq r \leq R_d$$

3. Mathematical formulation

The computational domain is presented in figure 4.

In order to reduce the CPU time we can ignore the melt height h_m(from $z = 0$) in the crucible [17].

The calculation domain starts at the top of the capillary tube at H_{cap},as shown in the schematic diagram of Fig.4. This is a good approximation provided that we include the melt height $h_m$into account for meniscus calculation [17].
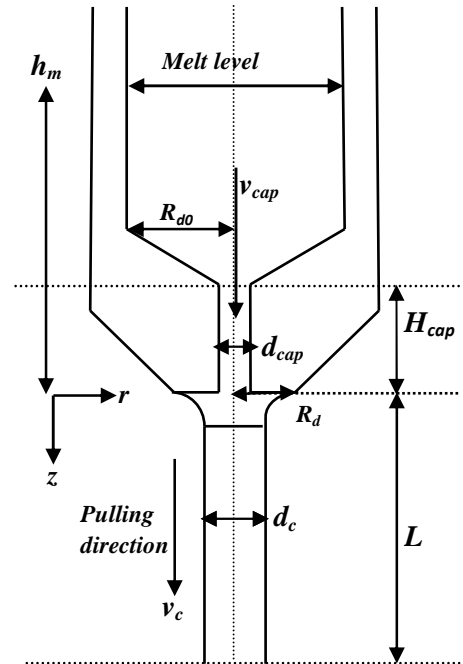

Fig.4: Schematic diagram of the computational domain.

3.1 Governing equations

The melt is assumed incompressible and Newtonian, while the flow is laminar. Dimensionless variables are defined by scaling lengths by R_d , velocity by α_m/R_d, temperature by the melting point T_m , and concentration by C_0, where α_m is the thermal diffusivity of the melt [17].

Because of the cylindrical symmetry of the problem, we have used a two dimensional axisymmetric model. The flow, the heat and the mass transfer are modeled by the dimensionless differential equations:

Equation of radial component of the momentum:

$$\frac{\partial u}{\partial t} + u\frac{\partial u}{\partial r} + v\frac{\partial u}{\partial z} =$$

$$-\frac{\partial p}{\partial r} + Pr\frac{\partial}{\partial r}\left(\frac{1}{r}\frac{\partial}{\partial r}(ru)\right) + Pr\frac{\partial}{\partial z}\left(\frac{\partial u}{\partial z}\right) (5)$$

Equation of axial component of the momentum:

$$\frac{\partial v}{\partial t} + u\frac{\partial v}{\partial r} + v\frac{\partial v}{\partial z} = -\frac{\partial p}{\partial z} + Pr\frac{\partial}{\partial r}\left(\frac{1}{r}\frac{\partial}{\partial r}(r\ v)\right) +$$

$$Pr\frac{\partial}{\partial z}\left(\frac{\partial v}{\partial z}\right) - PrRa_T T + \frac{Pr^2}{Sc}Ra_s C \qquad (6)$$

Conservation equation:

$$\frac{\partial \rho}{\partial t} + \frac{1}{r}\frac{\partial(r\rho u)}{\partial r} + \frac{\partial(\rho v)}{\partial z} = 0 \qquad\qquad (7)$$

Energy equation:

$$r\frac{\partial T}{\partial t} + \frac{\partial}{\partial r}(ruT) + \frac{\partial}{\partial z}(rvT) =$$

$$\frac{\partial}{\partial r}\left(r\alpha_i\frac{\partial T}{\partial r}\right) + \frac{\partial}{\partial z}\left(r\alpha_i.\frac{\partial T}{\partial z}\right) \qquad i = (m, c) \quad (8)$$

Dopant concentration equation:

$$r\frac{\partial C}{\partial t} + \frac{\partial}{\partial r}(ruC) + \frac{\partial}{\partial z}(rvC)$$

$$= \frac{P_r}{Sc}\left[\frac{\partial}{\partial r}\left(r\frac{\partial C}{\partial r}\right) + \frac{\partial}{\partial z}\left(r\frac{\partial C}{\partial z}\right)\right] (9)$$

Fig.5 shows the mesh grid which has been used to solve numerically the above equations. The physical domain in axisymmetric cylindrical coordinates (r,z) was subdivided into a finite number of contiguous volumes (CV) of volume V ,which are bounded by cell faces located about halfway between consecutive nodal points. This subdivision has been used for tow phase of sapphire (*i=m* for the melt, *i=c* for the crystal.)
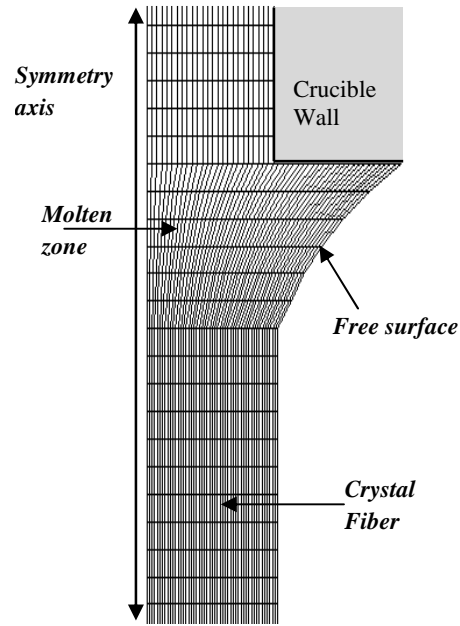

Fig. 5: *A portion of a sample mesh for calculation.*

3.2 Boundary conditions

It is assumed that the solute is uniformly distributed in the melt reservoir and its concentration is C_0; also the solute diffusion in the solid phase is neglected[18]. These governing equations with their associated boundary conditions are discredited by a finite volume method (FVM). We present below a detailed description about the boundary conditions simulations as the reference [17].

3.2 .1 Boundary conditions at the symmetric axis

In our two dimensional axisymmetric model the boundary condition at the symmetric axis for the physical quantities is set as follows:

$$\frac{\partial \Phi}{\partial r} = 0$$

In the above equations, Φ is the physical propriety (velocities$u$, v, temperature T, concentration$C$).

At the other boundaries the conditions were set for each physical quantity as follows:

3.2 .2 Temperature boundary conditions

- At the top entrance the temperature was set by the radio frequency generator. It's about$\Delta T \approx 20$ to $30\,K$ above the melting point of sapphire.

$$T = T_m + \Delta T \qquad\qquad (10)$$

-At the material surface, the heat transfer from the system to the ambient is controlled by convection according to the energy balance along the material surface:

$$n. k_i \vec{\nabla} T = -Bi(T - T_a) \qquad (12)$$

Where **n** is the unit normal vector on the melt or crystal surface pointing outwards; k_i is the ratio of thermal conductivity of phase i to the melt; where ($i = m(melt), i = c(crystal)$ and $Bi = hR_d/k_m$ is the Biot number. In this study the ambient temperature T_a is set to be a constant.

- At the end of the fiber $z = L$ using the fixed-temperature boundary condition, i.e. $T = T_a$.

3.2.3 Velocity boundary conditions

-The radial and axial velocities at the top entrance are given as follows:

$$u = u_0 = 0$$

$$v = v_{cap} = \left(\frac{\rho_c}{\rho_m}\right)\left(\frac{d_c}{d_{cap}}\right)^2 v_c (13)$$

Where v_c is the growth velocity, and v_{cap} is the flow velocity in capillary channel

-At the wall inside the capillary,

$$u = 0$$

$$v = 0$$

- In the free surface, the two components of the velocity are deduced from Marangoni convection; where the tangential stress balance is required:

$$ns: t = Ma(s. \nabla T) \qquad (14)$$

Where s is the unit tangent vector at the free surface, Ma is the Marangoni number and **t** the shear stress tensor.

- In the crystal, velocity boundary condition is:

$$v = v_c$$

3.2.4 Solute concentration boundary conditions

At the top entrance $\left(z = -H_{cap}\right)$, the solute boundary condition is given by the solute flux balance:

$$\vec{e}_z. \vec{\nabla} C = \left(\frac{Sc}{Pr}\right) Pe_m(C - 1) \qquad (15)$$

Where e_z is the unit vector along the z axis, and ∇C is the gradient of the concentration.

-The Neumann condition is imposed at the melt/crystal interfaces:

$$\vec{n}. \vec{\nabla} C = \left[\left(\frac{\rho_c}{\rho_m}\right) - K\right]\left(\frac{Sc}{Pr}\right) Pe_c C(n. e_z) \qquad (16)$$

Where **K** is the segregation coefficient according to the phase diagram, and $\vec{n}$ is the unit normal vector at the growth front pointing to the melt, $Pe_m = v_m R_d/\alpha_m$ and $Pe_c = v_c R_d/\alpha_m$ are the Peclect numbers of the melt and crystal respectively.

4. Results and Discussion

In this study, we have fixed the concentration of titanium in the melt to 0.1 at% [19].
The physical properties of Ti³⁺: Al₂O₃ [15, 18 and 19] and some input parameters [17, 19] for calculations are listed in Table 1:

Table 1

Physical properties

$Cp_c = 1300 \ (J/KgK)$

$Cp_m = 765 (J/KgK)$.

$D = 5 \times 10^{-9} (m^2 /s)$

$k_c = 17.5 \quad W/mK$

$k_m = 3.5 \quad W/mK$

$\partial\gamma/\partial T = (-3.5) \times 10^{-5} Nm^{-1} K^{-1}$

$\mu_m = 0.0475 \quad Kg/ms$

$T_m = 2323 \qquad K$

$\Delta H = 1.1 \times 10^6 J/Kg$

$\beta_T = 1.8 \times 10^{-5} K^{-1}$

$\rho_c = 3960 \qquad Kg/m^3$

$\rho_m = 3500 \qquad Kg/m^3$

$K = 1$

$\phi_0 = 17^0$

Input parameters

$R_c = 0.3 - 1 \ mm$

$R_{cap} = 0.27 - 0.5 \ mm$

$R_d = 0.57 - 2 \ mm$

$C_0 = 0.1 - 0.2 \ at\%$

$v_c = (0.3, \ 0.5, \ 0.8 \ and \ 1) mm/min$

4.1 Effect of the pulling rate

4.1.1 The axial pulling rate

Our simulation focuses on the effect of the pulling rate on the homogeneity of titanium concentration along the growth fiber axis (radial and axial axis).
First, we present the axial distribution of Ti^{3+} concentration in the sapphire crystal fiber for different pulling rates; these results are illustrated in Fig.6.
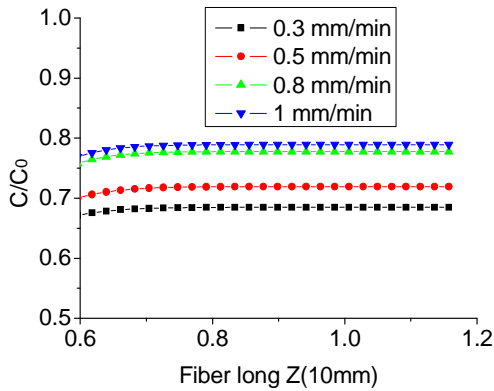

Fig.6: Titanium distribution along the axis of the sapphire fiber a function of pulling rate.

According to these results (Fig.6), we noticed that the longitudinal distribution of the Ti^{3+} remains homogeneous along the axis of the fiber even for relatively high pulling rates compared to other growth techniques [2].
The high pulling rate is one of the favorable conditions for axial homogeneous dopants distribution for the micro-pulling-down growth technique [12]. This result is in good agreement with experimental results of the dopants axial distribution reported in Fig.7.
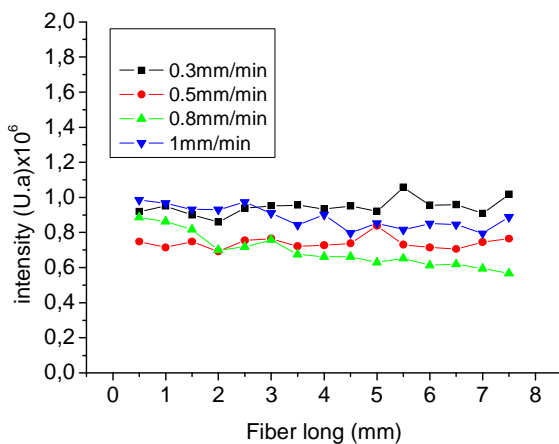

Fig.7: Titanium distribution along the axis of the fiber. Experimental: A. Laidoune.

Experimental results in Fig.7 show the homogeneity of Ti^{3+} along the longitudinal fiber direction for different pulling rates [19]. This result confirms the validity of our two-dimensional axisymmetric finite volume model.

4.1.2 The radial pulling rate

In figure 8, we present the radial distribution of Ti^{3+} for different pulling rates.
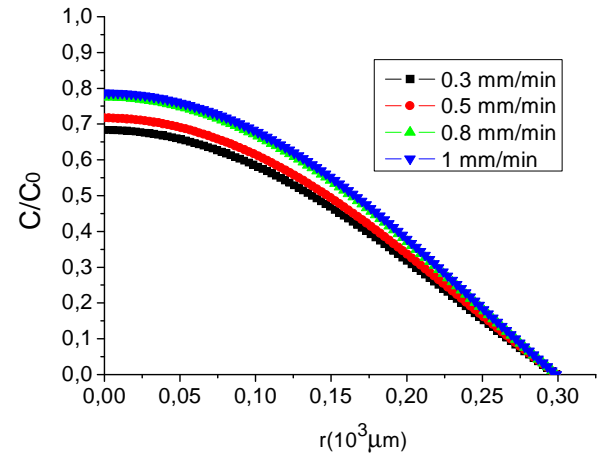

Fig.8: Ti radial distribution for different pulling rate.

According to these results (Fig.8), we observed that the radial distribution of Ti dopants gather around the axis of the fiber. Thus there is no segregation towards the periphery. This result remains true for relatively high pulling rates. Therefore these results confirm that the size and the geometry of the μ-PD growth technique helps to avoid the segregation of titanium towards the periphery of the fiber despite the high pulling rates used for this technique compared with other methods [1, 2].
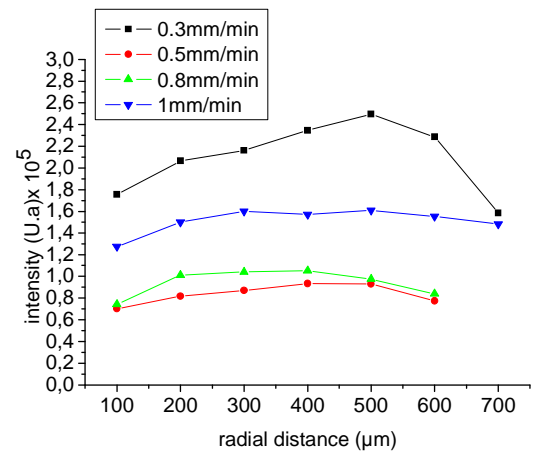

Fig.9: Luminescence measurements showing the titanium radial distribution.

Fig.9 presents the radial micro luminescence results that show the gathering of Ti^{3+} ions in the core of the fiber than in the periphery; the radial distribution is suitable as an amplifying medium for the design of fiber lasers [19].

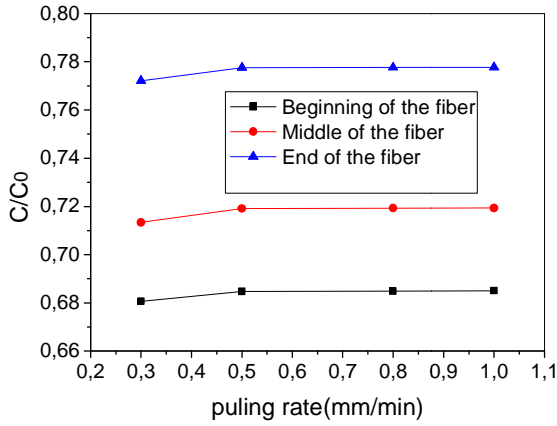*4.2.3 The variation of titanium concentration versus the pulling rate*

Fig.10: The concentration of titanium in the fiber as a function of the different pulling rate for three parts of the fiber.

Fig.10 shows the longitudinal homogeneity of the concentration of titanium along the fiber axis in good agreement with the experiment results obtained from the luminescence measurements of Fig.11 [19]:
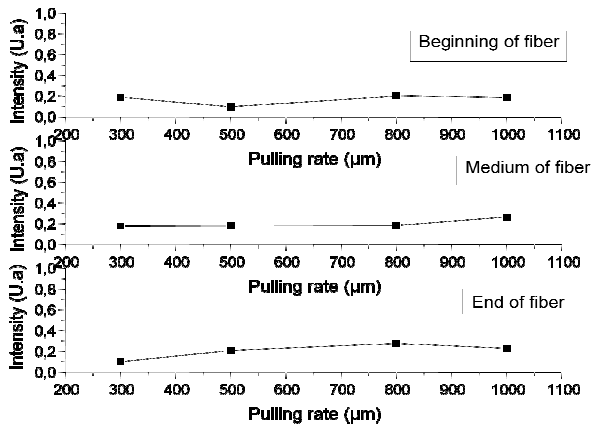

Fig.11: Luminescence measurements showing the concentration of dopants in three parts of the fiber as function of the different pulling rate.

4.2 The melt/crystal interface shape

The quality of the crystals and single crystal fibers is governed by many factors, citing the dynamics of drawing, the thermal transfer, effect of convection, and the geometry of the melt/crystal interface.

The melt/crystal interface shape plays an important role for the quality of the crystal fiber drawn. The shape of this interface is essentially determined by the heat transfer in the growing system [20].
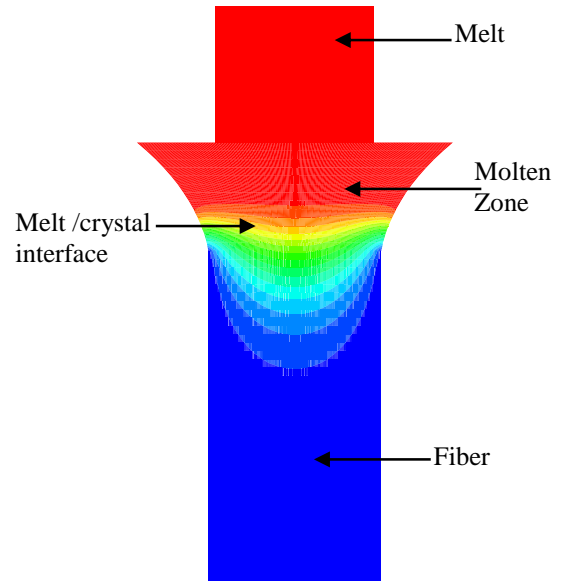

Fig.12: Temperature contour plot showing the melt/crystal interface.

Fig. 12 shows the temperature contour plot (heat transfer) in the growth system. The blue color is the solid and the red color is the sapphire melt. According to these results, the melt/crystal interface for the μ-PD technique has almost a flat shape and this is in good agreement with the experiment observation [19]. This flatness of the interface shape is very important since it shows that drawing conditions are very stable.

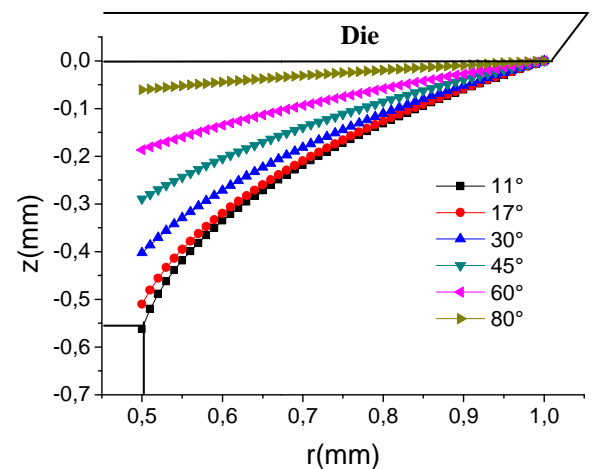*4.3 Effect of growth angle on the height of the molten zone*

Fig 13: The variation of the height of the molten zone as function of the growth angle.

The meniscus shape is mainly affected by the capillary shape and the melt height [17]. In this part we have studied the effect of the growth angle on the meniscus shape also on the height of the molten zone on the meniscus shape and on the height of the molten zone. Fig.13 shows the calculated meniscus shapes for different growth angle: (11°, 17°, 30°, 45°, 60° 80°).

We noticed that the height of the molten zone decreases when the angle of growth increases. As results the decrease or the increase of the meniscus height causes an increase or decrease in the diameter of the fiber [19], and this affects on the quality of the drawn fiber.

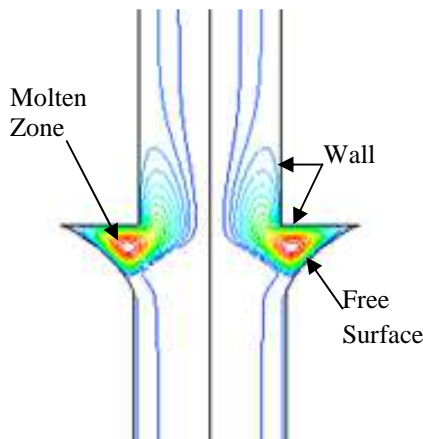*4.4 Effect of the geometry of the µ-PD technique on the segregation problem*

Fig 14: Presentation of streamline in the µ-PD technique.

According to Fig 14, we notice that there is no flow near the free surface and the wall (blue color). This is one of the advantages of this method over other growing methods It is related to the small dimensions (mm, µm) involved in the micro pulling process.

So the size of the micro-pulling down avoids and minimizes the segregation problem of the dopants towards the periphery. Because the laser beam passes in the axis of the fiber, this result show that the use of this technique reduces significantly the segregation towards the periphery of the fiber making the large concentration of Ti^{3+} in the center of the core of the fiber where it is needed.

In fact the experimental and the simulation results show that the micro pulling down geometry helps to avoid the dopants' segregation which is great advantages to pull performed materials single crystals fiber with good optical and thermal properties.

5. Conclusion

In this work we have established a two-dimensional axisymmetric finite volume model (FVM) in cylindrical coordinates to study the growth of Ti: Al_2O_3 material by the µ-PD technique. This study shows:

- With other growing techniques we usually observe the segregation of the dopants towards the periphery. Whereas for the micro pulling down technique we showed that the dopants distribution of Ti^{+3} is homogeneous whatever the pulling rate and there is no segregation towards the periphery.

- The longitudinal mass transfer (longitudinal distribution of the Ti^{3+}) remains homogeneous along the axis of the sapphire fiber even for relatively high pulling rates; this homogeneity gives a material with a good optical and thermal quality for several applications [19]. Our results are in good agreement with experimental results that show that the obtained fibers have a good morphological and optical quality [19].

- The radial mass transfer of titanium increase in the crystal drawn when the pulling rate increases.

- The heat transfer gives information on the shape of the melt/crystal interface; which plays an important role for the optical and thermal quality of the material drawn.

- The size and the geometry of the crucible and the pulling rate minimize the segregation problem of the dopants to the periphery of the fiber. This is due to the fact that the dopants do not have enough time to migrate to the periphery during the growth.

- Our results are in good agreement with the experiment that show that the obtained fibers have a good morphological and optical quality and. This agreement shows the validity of the two-dimensional axisymmetric finite volume model.

Therefore, for the micro pulling down (µ-PD) method, the results obtained are important for laser applications. Indeed, for other growth methods such as Czochralski [6], it is not easy to avoid the problem of segregation to the periphery, whereas the micro pulling down promotes the gathering of impurities towards the axis of the fiber making a good overlap with the laser beam when the material or the fiber is used as amplifying medium in a laser.

References

[1] Fukuda T., Advances IN materials Research 8, 2007.

[2] THIERRY DUFFAR. © 2010 John Wiley & Sons Ltd.

[3] Chandra P. Khattak, Frederick Schmid, Journal of Crystal Growth. 225 (2001).

[4] G. Alombert-Goget, K. Lebbou, N. Barthalay, H. Legal, G. Chériaux. Optical Materials 36 (2014) 2004-2006.

[5] H. Li, E.A. Ghezal, G. Alombert-Goget, G. Breton, J.M. Ingargiola, A. Brenier, K. Lebbou. Optical Materials 37 (2014) 132-138.

[6] Reinhard Uecker ; Detlef Klimm ; Steffen Ganschow ; Peter Reiche ; Rainer Bertram ; Mathias Roßberg ; Roberto Fornari. Proc. SPIE 5990, Optically Based Biological and Chemical Sensing, and Optically Based Materials for Defence, 599006 (October 15, 2005).

[7] David B. Joyce, Frederick Schmid. Journal of Crystal Growth 312 (2010) 1138-1141.

[8] A. A. Anderson, R. W. Eason, L. M. B. Hickey, M. Jelinek, C. Grivas, D. S. Gill, and N. A. Vainos, Optics Letters 22, 1556-1558 (1997).

[9] L. S. Wu, A. H. Wang, J. M. Wu, L. Wei, G. X. Zhu, and S. T. Ying, Electronics Letters 31, 1151-1152 (1995).

[10] E. A. Ghezal, H. Li, A. Nehari, G. Alombert-Goget, A. Brenier, K. Lebbou, M. F. Joubert, and M. T. Soltani, Crystal growth & design. 12 (2012) 4098-4103.

[11] D.Sangla, N.Aubry, A.Nehari, A.Brenier, O.Tillement, K.Lebbou , F.Balembois,. Journal of Crystal Growth 312(2009)125-130.

[12] A. Nehari, T. Duffar, E.A. Ghezal, K. Lebbou. Cryst. Growth Des.2014, 14, 6492-6496.

[13] V.A. TATARCHENKO and G.A. SATUNKIN. Journal of Crystal Growth 37 (1977) 285—288.

[14] T. SUREK, B. CHALMERS and A.I. MLAVSKY. Journal of Crystal Growth 42 (1977) 453—465.

[15] H. S. Fang, Z. W. Yan, and E. D. Bourret-Courchesne. DOI: 10.1021/cg101021t .2011. CRYSTAL GROWTH & DESIGN Article. Vol. 11, 121 129.

[16] V.A. Tatarchenko. Journal of Crystal Growth 37 (1977) 272.

[17] C.W. Lan, S. Uda, T. Fukuda. Journal of Crystal Growth 193 (1998) 552Ð562. June 1998.

[18] Abdeldjelil Nehari . THESE DE DOCTORAT L'UNIVERSITE DE LYON 2011.

[19] A. Laidoune. Thèse de doctorat. Université Hadj de Lakhdar - Batna, 2010 Algeria.

[20] Chung-Wei Lu, Jyh-ChenChen, Chien-HungChen (2010),. Journal of Crystal Growth 312; 1074-1079.

[21] Azoui. H, Laidoune. A, Djamel. Haddad, Bahloul. D. 3ème conférence Internationale des énergies renouvelables CIER - 2015 Proceedings of Engineering and Technology – PET pp.228-236 Copyright IPCO-2016.